Spectroscopic evaluation and fluorescence dynamics of several erbium doped laser materials
by Bruce Farris

A dissertation submitted in partial fulfillment of the requirements for the degree of Doctor of Philosophy in Chemistry
Montana State University

Abstract:
Spectroscopic analysis and kinetic modeling of relaxation processes have been completed for 2.1% and 4% Er:YAG, 2% Er:YSO, and 0.5% Er:LuAG at room temperature. Simultaneously time and frequency resolved emission spectra were obtained using step scan Fourier transform spectroscopy. Experimental emission lifetimes of the 4I13/2, 4I11/2, and 4S3/2 levels were obtained directly from these spectra. The 4I13/2 lifetimes were found to be 6.6, 6.5, 8.6, and 5.7 msec for 2.1% and 4% Er:YAG, 2% Er:YSO, and 0.5% Er:LuAG, respectively. Lifetimes of 67.3, 10.5, and 67.7 μsec were observed for 4% Er:YAG, 2% Er:YSO, and 0.5% Er:LuAG, respectively for the 4I11/2 state. Experimental lifetimes of 10.7, 3.5, and 12.3 μsec were observed for the 4S3/2 state in 4% Er:YAG, 2% Er:YSO, and 0.5% ErrLuAG.

Quantum-mechanical calculations using Morrison's code were performed and theoretical radiative rates were generated. Comparison of these values with experimental emission lifetimes allowed determination of non-radiative relaxation rates and branching ratios.

Additionally, an experimentally based new method of determining non-radiative rates was developed that utilizes the intensity "volume" under the three-dimensional emission bands. The two methods provided good agreement.

Finally, the rate constants obtained by these methods were plugged into a set of coupled differential equations and. numerically solved using the fifth order Runge-Kutta method in Mathematica. Good agreement with the experimental temporal behavior was obtained (including emission rises as well as decays) indicating the validity of the results. Non-radiative vs. radiative branching ratios were approximately equal for the first excited state 4I13/2, but higher electronic states typically showed > 99% of the population relaxing via the non-radiative channel.

SPECTROSCOPIC EVALUATION AND FLUORESCENCE DYNAMICS OF SEVERAL ERBIUM DOPED LASER MATERIALS

by

Bruce Farris

A dissertation submitted in partial fulfillment
of the requirements for the degree

of

Doctor of Philosophy

in

Chemistry

MONTANA STATE UNIVERSITY
Bozeman, Montana

July 2001

APPROVAL

of a dissertation submitted by

Bruce Farris

This dissertation has been read by each member of the dissertation committee and has been found to be satisfactory regarding content, English usage, format, citations, bibliographic style, and consistency, and is ready for submission to the College of Graduate Studies.

Lee Spangler — (Signature) — Date 7/18/01

Approved for the Department of Chemistry

Paul Grieco — (Signature) — Date 7-15-01

Approved for the College of Graduate Studies

Bruce McLeod — (Signature) — Date 7-23-01

STATEMENT OF PERMISSION TO USE

In presenting this dissertation in partial fulfillment of the requirements for a doctoral degree at Montana State University, I agree that the Library shall make it available to borrowers under rules of the Library. I further agree that copying of this dissertation is allowable only for scholarly purposes, consistent with "fair use" as prescribed in the U.S. Copyright Law. Requests for extensive copying or reproduction of this dissertation should be referred to Bell & Howell Information and Learning, 300 North Zeeb Road, Ann Arbor, Michigan 48106, to whom I have granted "the exclusive right to reproduce and distribute my abstract in any format in whole or in part."

Signature 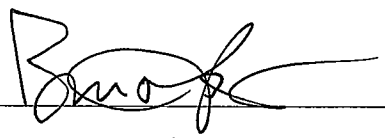

Date 19 July 2001

ACKNOWLEDGEMENTS

I would first like to thank my advising professor, Dr. Lee Spangler, for his support of my graduate study. Not only did he serve as an excellent teacher and research mentor, but he demonstrated extraordinary flexibility and support as I completed this work after accepting an opportunity to teach at Lansing Community College in Michigan. I would also like to thank the other members of my committee; Professors Edwin Abbott, Patrik Callis, Rufus Cone, Jack Riesselman, and Jan Sunner. This work would not have been possible without the other members of the Spangler research group; particularly Rich Martoglio, Tony Smith, and Wendi Sonnenberg for their involvement in other phases of the project. Additionally, I would like to express my gratitude to Dr. Reed Howald for his help and guidance on the kinetics portion of this work. Thank you to Dr. Michele McGuirl for the friendship and opportunity to discuss the project with a scientist that was not familiar with my work, providing a valuable perspective.

Also, I would like to thank my parents, Joe and Wiletta Farris, and my parents-in-law, Merle and Bonnie Johnson, for their support during my time in Montana. Thanks also to Benny Farris for motivating me to get away occasionally for much needed "sanity breaks"! Most of all, I'd like to thank my wife, Leslie, for her help, support, and extraordinary patience while I was completing this work.

TABLE OF CONTENTS

LIST OF TABLES

LIST OF FIGURES

ABSTRACT

Spectroscopic analysis and kinetic modeling of relaxation processes have been completed for 2.1% and 4% Er:YAG, 2% Er:YSO, and 0.5% Er:LuAG at room temperature. Simultaneously time and frequency resolved emission spectra were obtained using step scan Fourier transform spectroscopy. Experimental emission lifetimes of the $^4I_{13/2}$, $^4I_{11/2}$, and $^4S_{3/2}$ levels were obtained directly from these spectra. The $^4I_{13/2}$ lifetimes were found to be 6.6, 6.5, 8.6, and 5.7 msec for 2.1% and 4% Er:YAG, 2% Er:YSO, and 0.5% Er:LuAG, respectively. Lifetimes of 67.3, 10.5, and 67.7 μsec were observed for 4% Er:YAG, 2% Er:YSO, and 0.5% Er:LuAG, respectively for the $^4I_{11/2}$ state. Experimental lifetimes of 10.7, 3.5, and 12.3 μsec were observed for the $^4S_{3/2}$ state in 4% Er:YAG, 2% Er:YSO, and 0.5% Er:LuAG.

Quantum-mechanical calculations using Morrison's code were performed and theoretical radiative rates were generated. Comparison of these values with experimental emission lifetimes allowed determination of non-radiative relaxation rates and branching ratios.

Additionally, an experimentally based new method of determining non-radiative rates was developed that utilizes the intensity "volume" under the three-dimensional emission bands. The two methods provided good agreement.

Finally, the rate constants obtained by these methods were plugged into a set of coupled differential equations and numerically solved using the fifth order Runge-Kutta method in Mathematica. Good agreement with the experimental temporal behavior was obtained (including emission *rises* as well as decays) indicating the validity of the results. Non-radiative vs. radiative branching ratios were approximately equal for the first excited state $^4I_{13/2}$, but higher electronic states typically showed > 99% of the population relaxing via the non-radiative channel.

CHAPTER 1

INTRODUCTION

Erbium has been found to be a useful and versatile active atom for a variety of laser applications. It is capable of lasing near 3 μm, a desirable wavelength for laser surgery, and around 1.7 μm in the eyesafe region (1,2). Lasing has also been achieved at several IR and visible wavelengths via upconversion processes (2-8). Erbium is often doped into solid-state crystalline hosts, which offer the benefits of durability, reliability, and convenience. For these reasons, there has been considerable interest in solid-state lasers using erbium as the active ion. Since the optical properties such as absorption and emission influence laser performance, spectroscopic investigation has been carried out on erbium in a wide variety of crystalline hosts (9-56). Additionally, lasing has been achieved in many solid state laser materials using erbium as the active lasing species. (2-11, 36, 45, 54-76).

Energy Levels in Erbium Laser Materials

Erbium, like all rare earth elements typically used as active lasing species, is most commonly incorporated into crystalline hosts in the trivalent

state. The resulting ground electron configuration of the Er^{3+} ion is a xenon-like electron structure with 11 additional electrons in the partially filled 4f orbitals ([Xe] $4f^{11}$). The energy level structure of the erbium ion in crystalline hosts results from the Coulombic interaction of the 4f electrons with the nucleus and with each other, spin orbit coupling, and the host crystal field (77). The energy levels of the free Er^{3+} ion result from the electrostatic interaction and spin orbit coupling. The Coulombic interaction yields ^{2s+1}L terms, which are further split into J states by the spin-orbit interaction. The resulting free ion energy level diagram with the $^{2s+1}L_J$ states is shown in Figure 1, which includes the ground $^4I_{15/2}$ state through the seventh excited state ($^4F_{7/2}$). In actuality, the levels shown in Figure 1 are not pure $^{2s+1}L_J$ states, due to mixing of the levels. Each of the levels referred to by the $^{2s+1}L_J$ term symbol has other states mixed in. As can be seen by examination of the diagram, the free ion level separation is typically thousands of wavenumbers and transitions between the free ion levels are in the visible and infrared regions of the spectrum.

The host crystal field further splits each $^{2s+1}L_J$ term into a manifold of Stark levels. The degeneracy of the $^{2s+1}L_J$ states is 2J+1, and this degeneracy is reduced by the crystal field splitting (77). The splitting is relatively small, with an overall manifold width of typically several hundred cm^{-1}, and a splitting between adjacent Stark levels of normally 50 - 100 cm^{-1}, due to the shielding of the 4f electrons from the host crystal field by the outer 5s and 5p

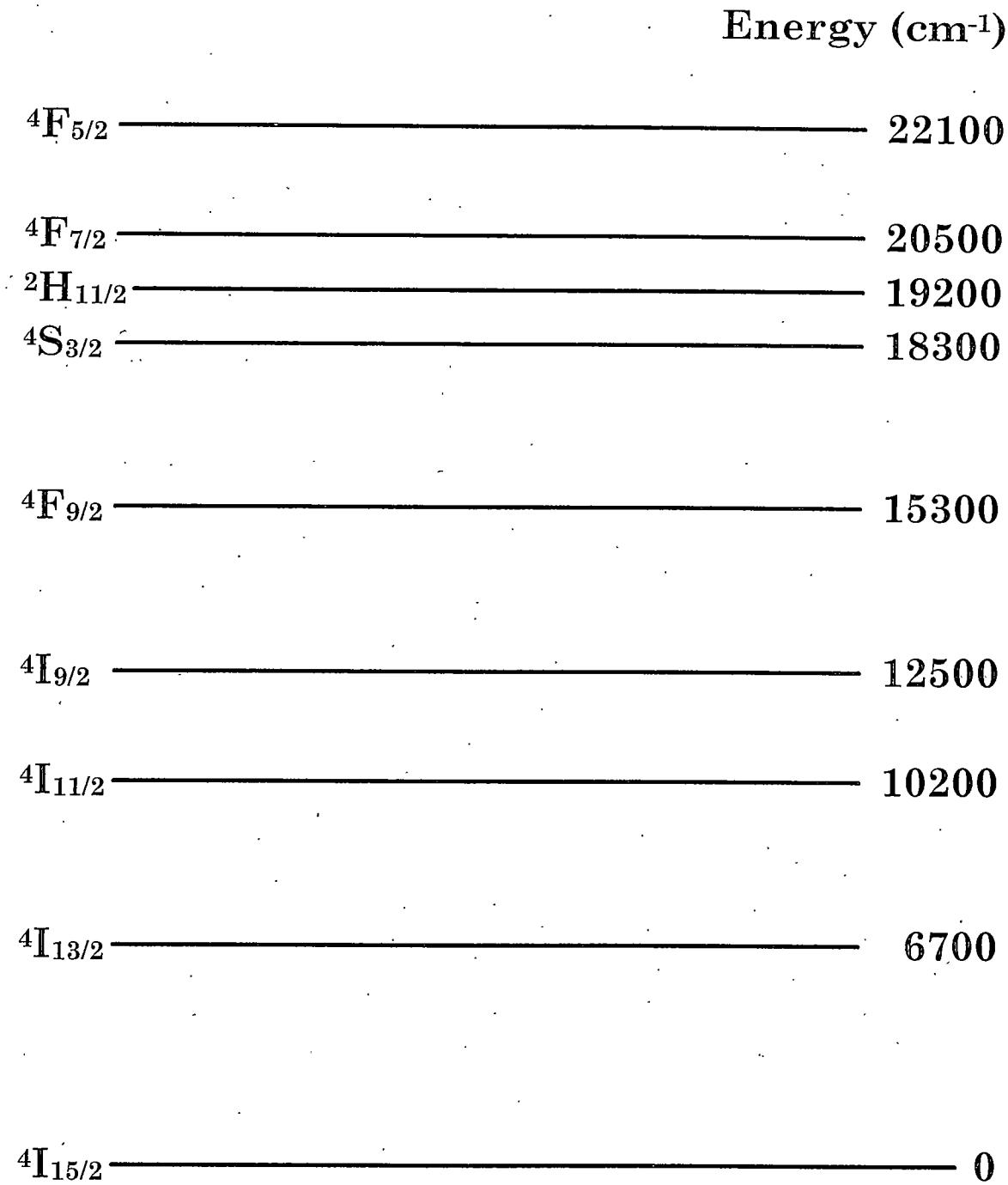

Figure 1. Free Ion Energy Levels for the Er^{3+} Ion.

electrons. The Stark level splitting can be exploited when a laser operating at a specific wavelength is desired. Coarse wavelength selection can be accomplished by choice of a specific rare earth ion, and fine "tuning" can be accomplished by selection of a host crystal that shifts the Stark levels such that the material is suited for the desired application. For that reason, Stark level assignment for different rare earth ions (including Er^{3+}) in crystalline hosts has historically been of interest, and a significant amount of work has been performed in this area for erbium(1,2,4,6,13,14,16,19-21,23,26,33,36,38-41,46,52,54,65).

Characterization of Laser Materials

The potential performance and operating characteristics of laser materials are to a large extent due to their spectroscopic properties. The absorption spectrum will determine potential pump wavelengths and influence pump efficiency, since pumping will be more efficient at strong absorption frequencies. After excitation has taken place, relaxation can occur via spontaneous radiative emission, nonradiative decay processes such as multiphonon relaxation, and/or ion-ion energy transfer processes. Radiative emissions can potentially be used as lasing transitions, and nonradiative

processes including energy transfer and multiphonon decay can enhance or detract from laser performance, depending upon the desired operating characteristics and pumping mechanism.

To ascertain the effect of the aforementioned properties on a particular lasing medium, it is useful to answer the following questions:

- What is the Stark level structure of the material?
- After excitation to a given manifold of Stark levels, what levels are involved in the relaxation process? Are these levels populated radiatively or nonradiatively? What levels are bypassed?
- Once populated, how is an excited state manifold depopulated? Is the manifold depopulated by radiative processes, nonradiative processes, or both? How quickly is it depopulated?
- What is the relative distribution (branching ratio) of the terminal levels of transitions originating from a particular manifold? What are the branching ratios of nonradiative relaxation processes?
- Do changes in dopant ion concentration (Er^{3+} in this study) or host crystal affect these population and/or depopulation processes?
- What, if any effects, are introduced by external factors such as temperature or excitation beam power?

Experimental methods or strategies that can answer some or all of these questions are of interest. Characterization of a material involves

absorption spectra, emission spectra resulting from continuous excitation to various manifolds, and temporally resolved emission spectra following modulated or pulsed excitation to the same manifolds. The absorption spectra are useful for determination of Stark level structure and identification of both excitation frequencies for emission experiments and pump frequencies for laser operation. The emission spectra provide information about the relaxation mechanisms from particular manifolds and identify promising laser transitions. The temporally resolved emission spectra provide information about the dynamics of both the radiative and nonradiative relaxation processes, which is of interest since the relative rates of population and depopulation of energy levels can affect whether and how well a material can function as a laser. For these reasons, these three experimental methods are all used in this study.

While spectroscopic study is useful in providing the previously mentioned information, combining it with complementary tools such as quantum-mechanical models and kinetic modeling using rate equations can increase its effectiveness. Emission spectra alone allow for direct observation of radiative emission transitions and provide some indirect information about nonradiative relaxation transitions. However, nonradiative relaxation rates and branching ratios can be gained by comparing experimentally determined lifetimes (which result from both radiative and nonradiative means of depopulation) with either low temperature or theoretically determined

radiative manifold lifetimes (which assume radiative processes are entirely responsible for depopulation). In this study, theoretical lifetimes are obtained from the quantum-mechanical model discussed in the next section. Alternatively, the rate and the relative contribution of the nonradiative relaxation processes can be determined by a newly developed method (presented in Chapter 4) that utilizes the intensity "volume" under the three dimensional emission bands of the temporally resolved spectra.

The kinetics of relaxation can be investigated by using the rate constants for the various relaxation processes (obtained by the experimental and/or theoretical methods discussed in the previous paragraph) following excitation to a particular level by solving sets of simultaneous rate equations for the involved energy levels. The combination of experimental methods, quantum-mechanical modeling, and kinetic modeling using rate equations can provide information that none of the three methods can provide alone, including information about processes that cannot be observed spectroscopically.

Quantum-Mechanical Model

A quantum-mechanical model developed by Morrison *et al* was used to calculate theoretical radiative lifetimes. The model is described in detail in Refs. 78-80 and is described briefly in this section.

Free ion wavefunctions are determined using a Hamiltonian that contains electrostatic, spin-orbit , and L^2 interactions (81). The host crystal field splits the free ion energy levels into Stark levels. Calculations of the Stark effects use a crystal field Hamiltonian of the form:

$$H_{CF} = \sum_i B_{nm} C_{nm}(i) \qquad (1)$$

where the B_{nm} are crystal field parameters which describe the effect of the host crystal field on the free ion energy levels, the C_{nm} are spherical tensor operator components, nm covers the values of n and m allowed by the symmetry of the site of the rare earth in the host crystal, and the i summation is over all of the 4f electrons of the rare earth ion. The crystal field parameters are related to the crystal field components A_{nm}, which are spherical tensor components of the host crystal field at the ion site, calculated by a point charge lattice summation. The A_{nm} and B_{nm} are related by the radial factor ρ_n, which are primarily functions of the rare earth ion, though they can be influenced slightly by the host crystal, and the relationships:

$$B_{nm}=\rho_n A_{nm} \qquad (2)$$

$$\rho_n = \frac{(B_{n0}^2 + 2B_{n2}^2 + 2B_{n4}^2 + \cdots)^{1/2}}{(A_{n0}^2 + 2A_{n2}^2 + 2A_{n4}^2 + \cdots)^{1/2}} \qquad (3)$$

Stark levels for a rare earth ion in a particular host crystal can be calculated entirely from the theoretical model. To do so, host x-ray data can be used to determine A_{nm} and Equation 2 can be used with the newly

determined A_{nm} to calculate the crystal field parameters B_{nm}. The calculated B_{nm} can then be used with Equation 1 used to determine the crystal field Hamiltonian. Alternatively, if experimental energy levels are known, a set of B_{nm} can be fit to the experimental data. The B_{nm} from the fit can then be used along with the A_{nm} for the host and Equation 3 to calculate ρ_n, which are then used with A_{nm} for a similar host and Equation 2 to calculate B_{nm} for the similar host. By the second method, experimentally determined Stark levels for a rare earth ion in one host can be fit and used to calculate Stark levels for the same ion in the other hosts from the same "family" (i.e. the garnets) providing better results than purely theoretical calculations (1). The Morrison model is limited to low dopant concentrations, as it does not include the effect of the rare earth dopant ion on the host crystal (which would change the point charge lattice summation and the A_{nm} values).

The model can also be used to calculate theoretical emission transition probabilities, which means that theoretical radiative lifetimes of a particular energy level can be obtained as well, using the Judd - Ofelt treatment (82,83). In this treatment, the Judd-Ofelt parameters Ω_k (which contain the host dependent part of the electric dipole line strengths) can be calculated (39,79) and used to calculate the theoretical electric dipole line strength $S_{ed}(J \rightarrow J')$. The magnetic dipole line strength $S_{md}(J \rightarrow J')$, which is entirely dependent on the rare earth ion within the theory, is calculated from the theoretical magnetic dipole oscillator strength. The line strengths for each transition of

interest can then be related to the Einstein A coefficients for the respective transitions.

CHAPTER 2

EXPERIMENTAL PROCEDURE

In this chapter, the overall approach to analysis of the materials, including types of spectra collected and justification for collecting them, will be explained. Next, the discussion includes a description of the analyzed samples and the equipment and techniques utilized in obtaining the various spectra. The chapter concludes with a brief discussion of the temporally resolved Fourier Transform spectroscopic technique used to gather most of the data.

Overall Method of Analysis

We are interested in the various population and depopulation processes (both radiative and nonradiative) of the energy levels in erbium-doped laser materials. The project goal was to use several spectroscopic techniques to gain relevant information about these processes. First, absorption spectra were collected for each sample. Although absorption spectra of laser materials are of fundamental interest since they provide information on potential pump wavelengths for laser use, the more

immediate and practical use for the purposes of this project was to provide appropriate excitation frequencies of the samples for collection of emission spectra. While absorption spectra for Er:YAG (4,6,26,34,35,37,38,46), Er:LuAG (9), and Er:YSO (34,36,39,40), are well documented in the literature, it was still beneficial to run absorption on the specific samples analyzed to account for any impurities or anomalies.

Two different emission techniques were employed in this project: standard emission and temporally resolved emission. The standard emission spectra were obtained using a continuous excitation source, but source modulation was necessary to obtain the temporally resolved spectra. The standard emission spectra were obtained much more rapidly and conveniently than the temporally resolved spectra and provided sufficient information to make them worthwhile, even though the spectral information was reproduced in the temporally resolved emission spectra. First, the continuously pumped emission spectra were useful for initial identification and assignment of emission bands and their relative contribution toward depopulating higher energy levels after excitation. Secondly, they provided information useful in the setting up of the temporally resolved spectra. The longer-lived emission bands typically appeared stronger in the continuous spectra, so some very rough qualitative information on emission band lifetime could be extracted. However, this information is by no means conclusive since actual emission transition intensity must also be considered.

Finally, identification of emission bands by continuous spectra facilitated the setting up of appropriate wavelength ranges for temporally resolved spectroscopy.

In addition to providing the above-mentioned information, the temporally resolved emission spectra provided emission decay rates and allowed the deconvolution of multiple overlapping bands which were difficult to distinguish in the spectral dimension. Second, since emission bands with the same decay profiles likely originate from the same manifold, it provided more convincing evidence for the assignment of emission transitions. Third, comparing emission spectra excited at different frequencies yielded information about the nonradiative processes involved in deexcitation. Finally, the ability to pump several excited states of the sample and observe the "turning on and off" of emission bands helped identify the originating manifold of the emission transitions. These capabilities will be demonstrated in Chapters 3 and 4.

Samples

Scientific Materials Corporation provided the erbium-doped YSO, YAG, and LuAG samples analyzed in this project. The samples were discs cut from crystals grown by Scientific Materials and polished on the edges and faces. They are approximately one-eighth inch thick and range from 0.5 to 1.5

inches in diameter. Erbium ions occupy yttrium sites in both the YAG and YSO crystal lattices, while they occupy lutetium sites in LuAG. There are two inequivalent sites occupied by erbium in Er:YSO, and the YSO host has three principal axes of polarization (39). While both orientationally resolved and unoriented absorption spectra were obtained for Er:YSO, orientationally resolved emission spectra were not obtained since it has been determined that the contribution of the two erbium centers to emission (on the time scales studied in this work) does not depend on which one is pumped more efficiently. (39) Moncorge *et al* found that the fluorescence bandshapes were identical for all the pump wavelengths studied (it is expected that for a particular wavelength one site would be excited more efficiently than the other), indicating that energy transfer occurs on a sufficiently faster time scale than the emission transitions studied, which occur on the microsecond and millisecond time scales.

Equipment and Techniques

The need to conduct the various experiments discussed earlier in this chapter makes a versatile spectroscopic facility necessary. The equipment and experiment setups used in this project are nearly identical to those described by Richard Martoglio (a previous member of the Lee Spangler research group at Montana State University) in his thesis (84) detailing his

similar work with thulium-doped materials. These procedures will be briefly outlined in this section, and all differences from the equipment setups described by Martoglio will be discussed in detail. A general equipment layout is shown in Figure 2.

Absorption

Absorption experiments were carried out using the Bruker IFS66 Fourier Transform Spectrometer. The instrument, which was described in detail by Martoglio (84), utilizes a Michelson interferometer as its basic design. The source was a broadband tungsten lamp included in the spectrometer. Two different beamsplitters were used depending on the spectral range desired for the specific experiment: a calcium fluoride beamsplitter was generally used for lower frequency measurements and a quartz beamsplitter was utilized for higher frequency spectra. A liquid nitrogen cooled indium antimonide detector was utilized in the infrared, while visible detection was accomplished using a silicon diode. Figure 3 shows response curves for all four possible detector/beamsplitter combinations. The detector/beamsplitter combinations for all absorption and emission experiments were chosen to get the best signal response for the desired spectral region.

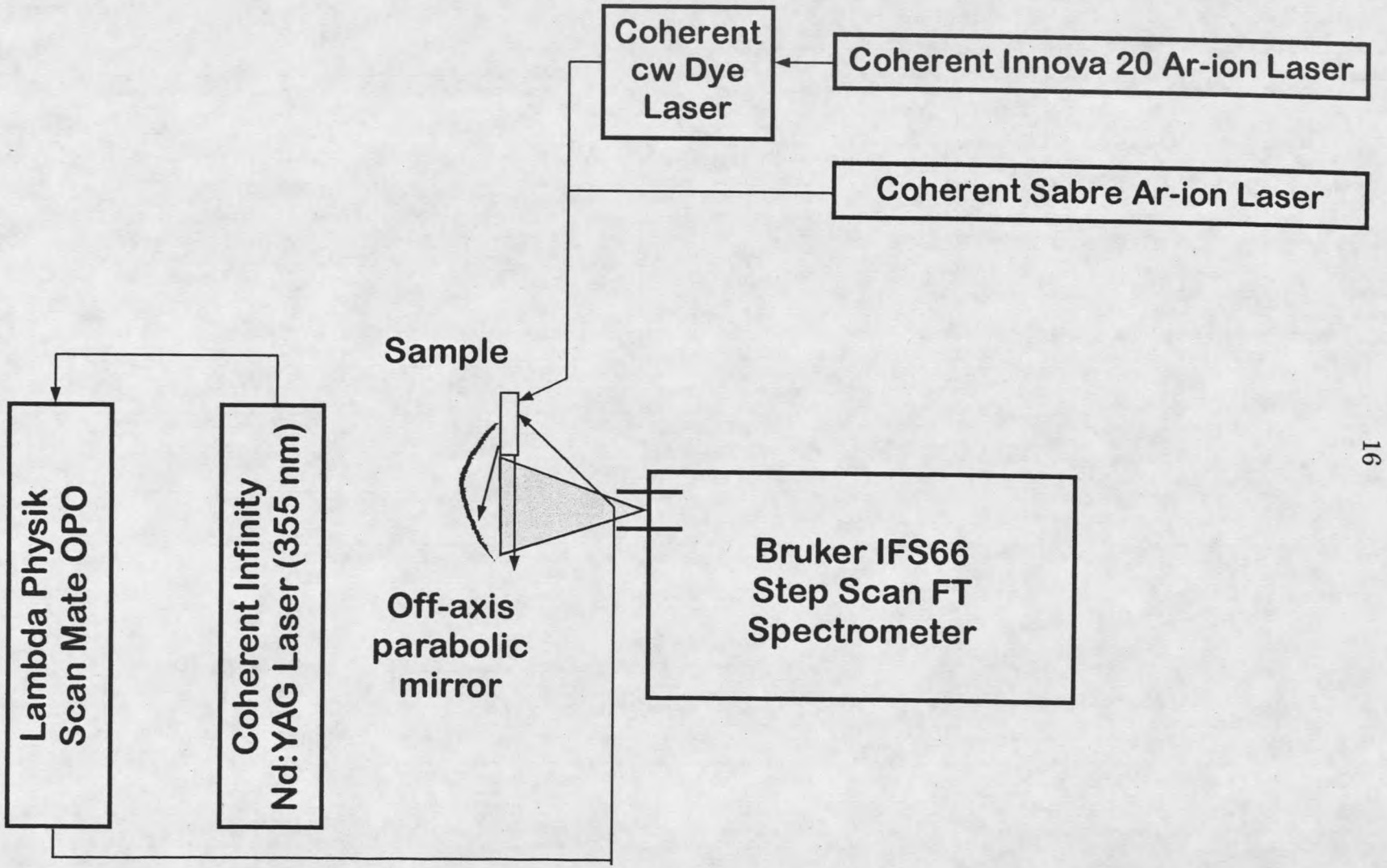

Figure 2. Experimental Set-up for Absorption and Emission.

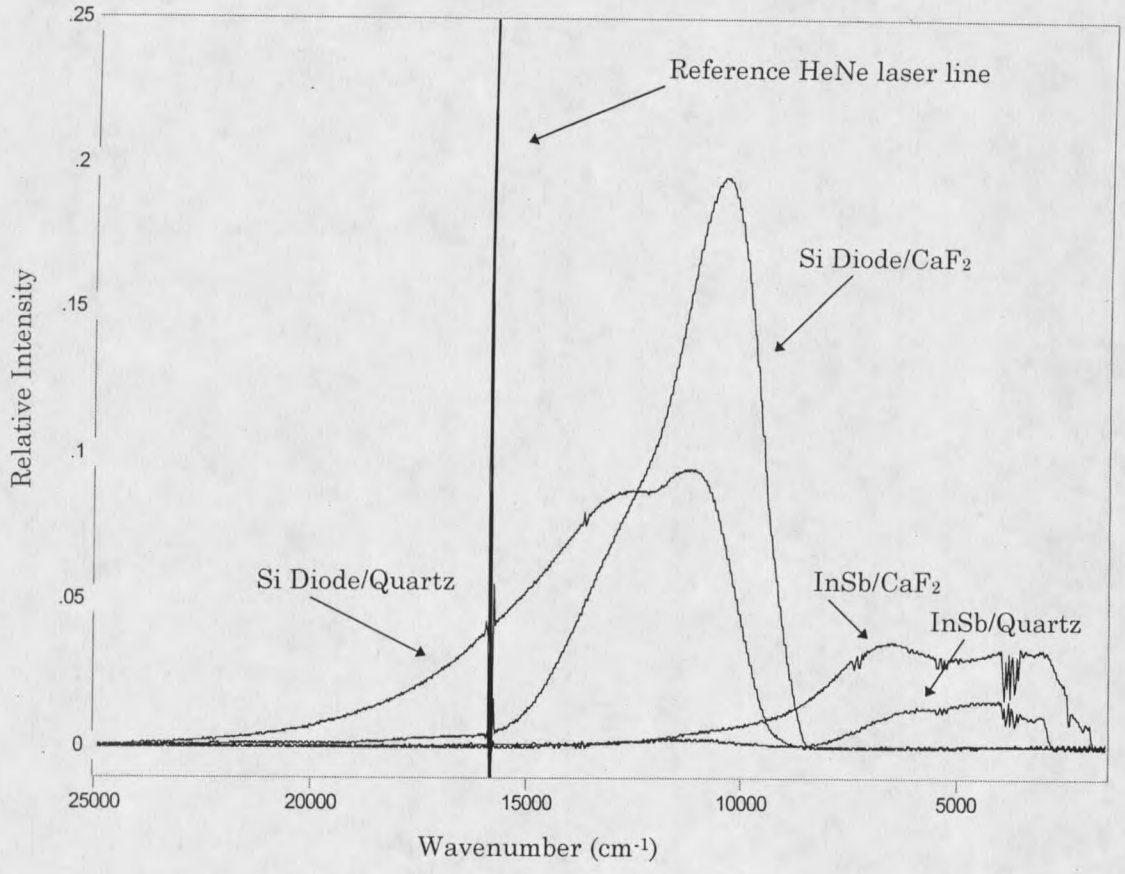

Figure 3: Response Curves for Detector/Beamsplitter Combinations.

Emission

An argon-ion laser provided a convenient excitation source for emission experiments since all the samples studied absorb the 488 nm line. Two different Ar-ion lasers were used as sources during the project. In addition to functioning directly as an excitation source, one of the Ar-ion lasers was also used to pump a Coherent continuous dye laser, allowing access to other erbium absorption bands.

The general emission setup is illustrated in Figure 2. After excitation by the Ar-ion laser, sample emission was collected by an off-axis parabolic mirror. The parabolic mirror was obtained from Bruker and was originally designed for light collection before entering the IFS66 spectrometer, thereby ensuring f-matching (f/4.5) to the IFS66. The sample was placed at the appropriate distance outside the interferometer to allow f-matching. Collecting the emission in the off-axis parabolic mirror improved emission signal-to-noise by a factor of approximately 40 over simply placing the sample in front of the IFS66 emission port, due to collection of a larger solid angle of the emitted radiation. Additionally, an aperture was sometimes placed at the IFS66 emission port to eliminate unwanted scattered laser light. The same beamsplitters and detectors used for absorption were used for the emission measurements, and optical filters were sometimes placed in the IFS66 absorption sample chamber to prevent unwanted emission signal and/or scattered source light from reaching the detector.

Temporally Resolved Emission

In this section, the equipment and setup for the temporally resolved emission experiments are discussed. The temporally resolved spectroscopic method is discussed in more detail in the next section.

Since source modulation was necessary to conduct the time-resolved experiments, the Ar-ion source (or Ar-ion pumped continuous dye laser) was

modulated using either a chopper (for millisecond pulses) or an acousto-optic modulator (for microsecond pulses) for the earlier experiments during the initial stages of the project.

A shorter excitation pulse was necessary to study the relaxation processes in these materials, many of which occur on the microsecond time scale or faster, thus nanosecond pulses were used for most of the temporally resolved work. The 1064 nm output from a Coherent Infinity Nd:YAG laser was tripled to 355 nm and used to pump a Lambda-Physik ScanMate OPO. The OPO could provide tunable output from 400 nm to nearly 2.5 microns, and output powers used were typically 2-5 mJ/pulse. With system repetition rates adjustable from 0.1 to 100 Hz, the Infinity/ScanMate combination provided the necessary flexibility to excite each different sample to a number of different electronic states. Additionally, the repetition rate could be set to allow for complete relaxation of the material before the next pulse was delivered.

The general experiment layout for the temporally resolved emission work was identical to the continuous emission setup (see Figure 2). When the Infinity/OPO excitation source was used, the beam was focused from approximately one cm to 2 mm in diameter using a f/12 lens (based on lens diameter) placed between the OPO outlet and the sample. The sample was placed at the focal point to maximize pump power density. Additionally, the sample placement was such that the excitation beam struck the sample near

the edge to minimize self absorption. The moving mirror in the Bruker interferometer was operated in step scan mode rather than rapid scan mode (this will be discussed further in the next section). Since the mirror was designed to be at a complete stop while gathering data, the system was susceptible to mechanical vibration. There are two major differences in the equipment setup used for gathering most of the time resolved data in this study with the setup employed by Martoglio. (84) First, the Infinity/OPO source was mounted on a larger optical table along with the interferometer. The optical table in use when Martoglio gathered his data was too small to accommodate the entire system. Tying the entire system together on one table greatly diminished the effect of building vibrations on the system, enhancing the signal-to-noise ratio. Additionally, the setup was moved to the Spangler group's temporary laboratory facility at Scientific Materials Corporation, which was located on the ground floor as opposed to the second floor laboratory in Gaines Hall at MSU. The overall building vibrations were less on the ground floor location, again providing improved mechanical stability and signal-to-noise ratio.

Temporally Resolved FT Spectroscopy

In this section, the temporally resolved Fourier Transform technique is briefly discussed. The technique is discussed in detail by Martoglio. (84)

In a standard Fourier Transform experiment using a Michelson interferometer, the moving mirror is scanned continuously on the order of 40 kHz, known as "rapid scan" mode. Temporal resolution at a given wavelength cannot be obtained in rapid scan mode because the mirror position changes during the course of the temporal event. However, operation of the IFS66 in step scan mode allows the user to obtain temporal information. In step scan mode, the moving mirror is stopped at each location and data is obtained. The method of obtaining data is illustrated on Figure 4. At each mirror position, the desired number of data points are obtained at a time interval corresponding to the desired temporal resolution. This process can be completed as many times as desired for signal averaging. Data corresponding to a particular mirror position is shown as a horizontal column in the first part of the figure. An interferogram is constructed using the data from each of the different mirror positions at one moment in time, known as a "time slice" (illustrated in the second part of Figure 4). This process is repeated for each of the time slices, resulting in a separate interferogram for each moment in time. The data needed for each of these interferograms is a vertical column in the first part of Figure 4. Each interferogram is then Fourier transformed to yield a spectrum for each time slice (last part of Figure 4), resulting in a temporally resolved emission spectrum.